

Synergistic Dynamical Decoupling and Circuit Design for Enhanced Algorithm Performance on Near-Term Quantum Devices

Yanjun Ji* and Ilia Polian†

*Institute of Computer Architecture and Computer Engineering,
University of Stuttgart, Pfaffenwaldring 47, 70569 Stuttgart, Germany*

(Dated: May 28, 2024)

Dynamical decoupling (DD) is a promising technique for mitigating errors in near term quantum devices. However, its effectiveness depends on both hardware characteristics and algorithm implementation details. This paper explores the synergistic effects of dynamical decoupling and optimized circuit design in maximizing the performance and robustness of algorithms on near term quantum devices. By utilizing eight IBM quantum devices, we analyze how hardware features and algorithm design impact the effectiveness of DD for error mitigation. Our analysis takes into account factors such as circuit fidelity, scheduling duration, and hardware native gate set. We also examine the influence of algorithmic implementation details including specific gate decompositions, DD sequences, and optimization levels. The results reveal an inverse relationship between the effectiveness of DD and the inherent performance of the algorithm. Furthermore, we emphasize the importance of gate directionality and circuit symmetry in improving performance. This study offers valuable insights for optimizing DD protocols and circuit designs, highlighting the significance of a holistic approach that leverages both hardware features and algorithm design for high quality and reliable execution of near term quantum algorithms.

I. INTRODUCTION

Near-term quantum devices (NISQ) [1] hold immense potential but face hurdles in accuracy and reliability due to inherent noise arising from environmental fluctuations, imperfect gate operations, and qubit interactions. Moreover, limitations in qubit count and connectivity restrict the complexity of achievable quantum circuits. Robust error mitigation techniques [2] are therefore crucial to unlock the full potential of NISQ devices. Dynamical decoupling (DD) [3–6] stands out as a powerful approach for NISQ devices due to its simplicity and low resource overhead. It mitigates decoherence errors by applying a carefully designed sequence of control pulses during idle periods of the qubits. These pulses effectively suppress the unwanted interaction between qubits and their environment, protecting the desired quantum state. DD has been demonstrated in various quantum systems including spins [7–12], superconducting qubits [5, 13, 14], and trapped ions [15]. The effectiveness of DD extends beyond decoherence suppression, as it can also mitigate crosstalk [13, 16] and coherent errors [17].

Numerous DD sequences have been developed, with prominent examples including the Carr-Purcell (CP) [18], Carr-Purcell-Meiboom-Gill (CPMG) [19], XY4 [20–23], KDD [24], and Uhrig dynamical decoupling (UDD) [25]. However, the effectiveness of different sequences varies significantly [26]. Prior work has shown that the CPMG sequence outperforms the CP sequence [4]. Additionally, higher-order sequences generally outperform lower order sequences [4, 26], but optimizing pulse intervals within

CPMG and XY4 sequences can achieve comparable performance [26]. In the context of the quantum approximate optimization algorithm (QAOA) [27–31], DD sequences like CP, CPMG, and XY4 significantly enhance performance, while KDD showed worse performance on IBM quantum processing units (QPUs) [32]. Combining DD sequences with pulse-level optimization in QAOA can further improve performance [32]. While DD sequences mitigate errors, these additional control pulses can also introduce errors such as gate infidelities or crosstalk. To address this trade-off, adaptive approaches have been explored [33], which estimate the potential benefit of DD for each qubit combination and selectively apply DD to the subset that offers the most benefit. Furthermore, recent work has explored the use of empirical learning schemes for enhancing DD effectiveness on quantum processors [34], leveraging data-driven techniques to optimize the implementation of DD sequences, leading to improved error suppression capabilities.

Despite extensive research on DD sequences, most studies neglect the crucial role of algorithm implementation details such as transpilation efficiency [35–38], circuit structure, and gate decompositions [39]. This work addresses this gap by examining the factors influencing DD sequence effectiveness, emphasizing the critical role of algorithm implementation details in enhancing overall performance. We focus on the CPMG sequence due to its well-established effectiveness, robustness [4], and good performance for QAOA on IBM QPUs [32].

The study explores how hardware characteristics and algorithm design affect the effectiveness of DD for error mitigation on near term quantum devices by analyzing different implementations of the QAOA on eight IBM QPUs. Our findings reveal an inverse relationship between the initial performance of the algorithm without DD and the effectiveness of DD. While DD generally

* yanjun.ji@informatik.uni-stuttgart.de

† ilia.polian@informatik.uni-stuttgart.de

enhances performance and robustness, circuits with inherently higher fidelity and shorter execution times benefit less from DD than those with lower initial performance. Moreover, factors such as hardware native gates of QPUs, chosen gate decomposition strategy, and optimization level can also influence the effectiveness of DD. Additionally, using gates with consistent directionality and maintaining circuit symmetry during design lead to improved performance. These findings emphasize the importance of a holistic approach that considers both hardware and software optimization for the successful execution of algorithms with DD on NISQ devices, providing valuable insights for optimizing DD protocols and designing more robust quantum algorithms.

The paper is structured as follows. Section II outlines the methodology, presenting the benchmark circuits and metrics used to evaluate algorithm performance. Hardware considerations and a proposed synergistic design approach combining both hardware and algorithmic factors are also described. Section III then analyzes results, exploring the impact of various hardware factors including circuit fidelity, schedule duration, and native gate sets, as well as algorithmic factors including different implementations, DD sequences, and optimization levels. Finally, Sec. IV discusses the key findings and concludes.

II. METHODOLOGY

We experimentally investigate the impact of hardware and algorithmic factors on the effectiveness of dynamical decoupling in superconducting quantum processes. Hardware factors, such as circuit fidelity, schedule duration, and native gate sets, define the fundamental capabilities of a quantum device. Conversely, algorithmic factors encompass the design choices made during algorithm implementation (specific sequence of quantum operations), error suppression strategy (selection of a DD sequence), and circuit optimization techniques. These algorithmic choices ultimately determine how efficiently the inherent capabilities of the hardware are utilized for optimal performance. Understanding these factors can potentially improve the practical implementation of algorithms on near term quantum devices.

A. Benchmark circuits and metrics

We first present benchmark circuits used in our demonstration and metrics employed to assess algorithm performance and DD effectiveness.

1. QAOA for portfolio optimization

We employ QAOA for portfolio optimization as benchmarks. The portfolio optimization problem aims to select

the optimal portfolio from all available options to maximize expected returns while minimizing financial risk. The QAOA has the potential to address this challenge [40–42]. The cost Hamiltonian, which describes the portfolio optimization problem for n available assets, is expressed as [41]

$$\hat{H}_c = \sum_{i=1}^{n-1} \sum_{j=i+1}^n c_{i,j} \hat{Z}_i \hat{Z}_j - \sum_{i=1}^n k_i \hat{Z}_i, \quad (1)$$

where $c_{i,j}$ and k_i are parameters specific to portfolio optimization, $\hat{Z}_i \hat{Z}_j$ and \hat{Z}_i represent ZZ interaction on qubits (i, j) and Pauli Z operator acting on qubit i , respectively. The mixer Hamiltonian is given by [27]

$$\hat{H}_m = \sum_{i=1}^n \hat{X}_i, \quad (2)$$

where \hat{X}_i is Pauli X operator acting on qubit i . After a QAOA depth of p , the total system evolves to $|\psi\rangle = \prod_{j=1}^p e^{-i\gamma_j \hat{H}_c} e^{-i\beta_j \hat{H}_m} |\psi_0\rangle$, where $|\psi_0\rangle$ is the eigenstate of the mixer Hamiltonian. The aim of QAOA is to find $2p$ parameters $(\beta_1, \dots, \beta_p, \gamma_1, \dots, \gamma_p)$ that minimize the expectation value of the cost Hamiltonian $F = \langle \psi | \hat{H}_c | \psi \rangle$. We define the approximation ratio of QAOA as

$$r = \frac{F - F_{\max}}{F_0 - F_{\max}}, \quad (3)$$

where F_0 represents the optimal value, and F_{\max} signifies the worst-case value.

Our study uses QAOA with qubit numbers ranging from 3 to 12 and a depth of 1. To establish a baseline for experimental results, we present the simulation results conducted in a noise-free environment with Qiskit's Qasm simulator in Table I. All data use 30000 circuit repetitions (shots). We observe that approximation ratio and success probability decrease as the number of qubits increases.

2. Metric definition

To quantify the impact of noise, we introduce two normalized metrics: the normalized approximation ratio (NAR) and the normalized success probability (NSP). These metrics are defined as

$$\text{NAR} = r_\epsilon / r_0, \quad (4)$$

$$\text{NSP} = p_\epsilon / p_0, \quad (5)$$

where r_ϵ and p_ϵ represent approximation ratio and success probability obtained under noise conditions. r_0 and p_0 denote corresponding values obtained from the simulated noise free case (Table I). For the same problem instances, we use identical values of r_0 and p_0 for evaluation. Due to noise, NAR and NSP typically exhibit

TABLE I. Noise-free simulation results of QAOA for portfolio optimization using Qiskit's Qasm simulator with 30000 shots.

Number of qubits	3	4	5	6	7	8	9	10	11	12
Approximation ratio	0.9751	0.4342	0.3776	0.3734	0.3589	0.3144	0.2806	0.3241	0.2933	0.3161
Success probability	0.9747	0.1536	0.1131	0.0422	0.0227	0.0124	0.0065	0.0057	0.0018	0.0006

values less than one. However, in rare instances, these metrics may exceed unity, indicating that specific noise patterns or randomness enhance performance compared to the simulated noise free case.

Without any error mitigation being applied, NAR and NSP for algorithms executing on real noisy quantum devices are given by

$$\text{NAR}_B = r_b/r_0, \quad (6)$$

$$\text{NSP}_B = p_b/p_0, \quad (7)$$

where B represents results obtained from real hardware without error mitigation. r_b and p_b represent the corresponding approximation ratio and success probability, respectively. When a specific error mitigation strategy, such as the DD sequence, is applied, NAR and NSP are given by

$$\text{NAR}_{\text{DD}} = r_d/r_0, \quad (8)$$

$$\text{NSP}_{\text{DD}} = p_d/p_0, \quad (9)$$

where DD denotes the application of DD sequences. r_d and p_d represent approximation ratio and success probability, respectively, with error mitigation. To assess DD effectiveness in error mitigation, we introduce two additional metrics: Δ_{NAR} and Δ_{NSP} . These metrics are defined as the difference between the corresponding values obtained with and without DD sequences:

$$\Delta_{\text{NAR}} = \text{NAR}_{\text{DD}} - \text{NAR}_B, \quad (10)$$

$$\Delta_{\text{NSP}} = \text{NSP}_{\text{DD}} - \text{NSP}_B. \quad (11)$$

A positive value for Δ_{NAR} and Δ_{NSP} indicates a successful improvement in performance resulting from the utilization of DD sequences.

We further introduce the concept of error mitigation success rate (EMSR) to quantitatively assess the robustness of an error mitigation strategy. EMSR is defined as the percentage of experimental trials in which the application of error mitigation resulted in a better outcome compared to the unmitigated scenario. A high EMSR indicates a high success rate associated with the error mitigation protocol. A value of 100% suggests that applying this error mitigation strategy consistently improves algorithm performance across all experiments. In contrast, a low EMSR value suggests that the effectiveness of error mitigation may not be universally applicable and could potentially diminish performance. In this study, we quantify the robustness of DD error mitigation with two metrics: EMSR_{AR} and EMSR_{SP} , depending on whether the approximation ratio or success probability is used. Any positive value of Δ_{NAR} contributes to an increase in

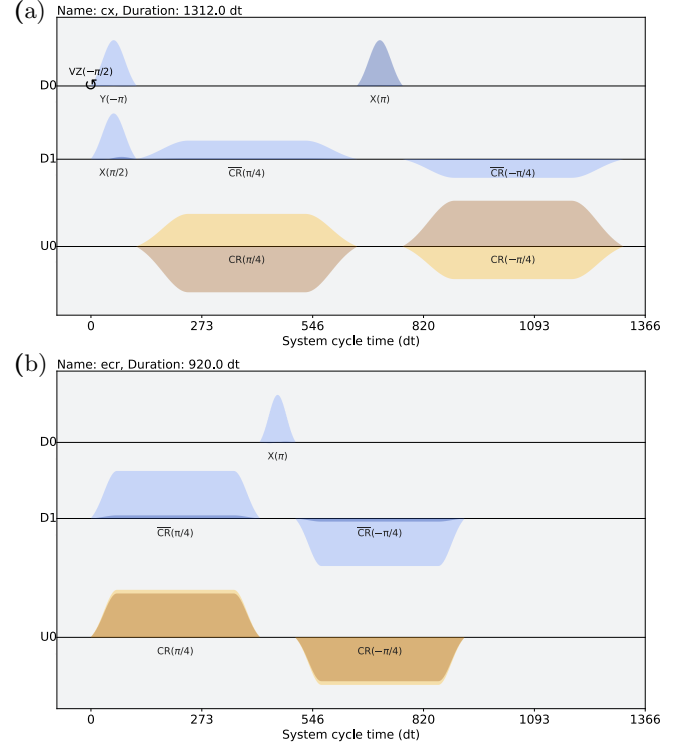


FIG. 1. Schedule of hardware native two-qubit gates: (a) CX gate on qubit pair (0,1) of ibm_cairo, and (b) ECR gate on qubit pair (0,1) of ibm_cusco. The system cycle time (1dt) is $2/9 \text{ ns} \approx 0.22 \text{ ns}$ in ibm_cairo, while it is 0.50 ns in ibm_cusco. D_i represents the drive channel acting on qubit i , and U_j is the control channel for a corresponding qubit pair (c, t) , driving the control qubit c at the frequency of the target qubit t .

EMSR_{AR} , while any positive value of Δ_{NSP} leads to an increase in EMSR_{SP} .

B. Hardware considerations

This section provides information about IBM quantum devices used in our experiments. The QPUs with 27 qubits, namely ibmq_mumbai, ibmq_kolkata, ibm_cairo, and ibmq_ehningen, operate using basis gates $\{\text{CX}, \text{ID}, \text{RZ}, \text{SX}, \text{X}\}$, where ID represents identity gate, RZ performs a single qubit rotation around the z -axis, X is the NOT gate, and SX is the square root of X. On the other hand, the QPUs with 127 qubits, specifically ibm_kyoto, ibm_cusco, ibm_brisbane, and ibm_sherbrooke, utilize basis gates $\{\text{ECR}, \text{ID}, \text{RZ}, \text{SX}, \text{X}\}$, where ECR is the echoed cross resonance gate.

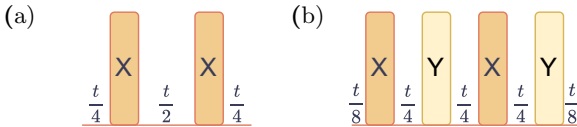


FIG. 2. Two types of DD sequences: (a) CPMG and (b) XY4. The delay time t represents the idle time of the qubit, minus the duration of the corresponding X or Y pulses.

Figure 1(a) illustrates the schedule of a native CX gate on `ibm_cairo`. This implementation employs a single pulse gate duration of 112 dt and a cross resonance (CR) gate duration of 544 dt, leading to a total duration of 1312 dt, where dt represents the system cycle time. In contrast, Fig. 1(b) depicts the schedule of a native ECR gate on `ibm_cusco`. Here, the single-pulse and CR gate durations are 88 dt and 416 dt, respectively, resulting in a shorter total duration of 920 dt. The CX gate is typically implemented using one ECR gate and multiple single qubit gates. A further decomposition of CX gate into ECR and single pulse gates at pulse level enables the elimination of single pulse gates during circuit optimization [43]. Additionally, CX-based IBM QPUs, where CX is the native gate, support the operation of CX in two directions. On the other hand, ECR-based QPUs, where ECR is the native gate, typically only support the ECR gate in one direction. Consequently, quantum circuits designed for these latter devices need to be decomposed into sequences of gates that include only the supported direction of the ECR.

C. Synergistic design approach

This section describes a synergistic design approach for maximizing the performance and robustness of algorithms on near term quantum devices. This approach acknowledges the critical interplay between the hardware's capabilities and the design choices made in the software implementation. The quality of algorithm implementation directly affects the performance. Key aspects include the efficiency of transpilation processes, specific gate types used, and the overall symmetry of the algorithm structure. For instance, studies have shown that the algorithm-oriented qubit mapping (AOQMAP) method [44] offers advantages in transpilation for variational quantum algorithms (VQAs) [45] compared to popular compilers such as Qiskit [46] and Tket [47] by introducing fewer two-qubit gates, maintaining a shallower circuit depth, and promoting higher symmetry [48].

In this study, we utilize the AOQMAP method [44] to efficiently map circuits onto hardware, aiming to minimize SWAP gates and circuit depth on linear topologies. Subsequently, we examine two implementations of QAOA for portfolio optimization on CX-based IBM

QPUs. These implementations differ in their choice of gate decompositions within the algorithms. The first implementation, referred to as the CX implementation, directly decomposes the gates in QAOA into basis gates of the QPUs using Qiskit's transpiler with optimization level 3. In comparison, the second implementation, referred to as the CZ implementation, initially decomposes gates in algorithms into CZ and single qubit gates. Then, Qiskit's transpiler with optimization level 3 is used to perform optimization and decomposition into basis gates of QPUs. Previous studies have demonstrated that this CZ decomposition approach outperforms CX decomposition for ZZ and ZZ-SWAP gates in QAOA on IBM QPUs [43]. During implementation, we also explore different optimization level settings in Qiskit and investigate their impact. To ensure consistency in evaluations, we employ identical benchmark circuits and parameters. Additionally, we consistently use 30000 shots for each demonstration. Within the Qiskit framework, we default to using optimization level 3.

We also investigate the effectiveness of two well-established DD sequences: CPMG and XY4. As illustrated in Fig. 2, the CPMG sequence applies two X pulses separated by a delay of $\frac{t}{2}$, with additional delays of $\frac{t}{4}$ at the beginning and end. The parameter t represents the time interval during which the qubit remains idle, excluding the duration of single qubit pulses, in the case of CPMG, two X pulses. In comparison, the XY4 sequence utilizes two X and two Y pulses, each separated by a delay of $\frac{t}{4}$, with additional delays of $\frac{t}{8}$ at the beginning and end. Additionally, the “alap” (as late as possible) scheduling method, which schedules the stop time of instructions as late as possible, is used for scheduling gates and inserting DD sequences throughout our study. Figure 3 showcases the resulting implementations of a three-qubit QAOA with CPMG sequence on a 27-qubit QPU `ibm_kolkata` using both CX and CZ implementations. Compared to CX implementation, CZ implementation employs all the same directed CX gates. Additionally, we observe an X gate inserted between control qubits of CX gates in the CZ implementation, potentially suppressing idle errors and improving performance. Moreover, CZ implementation shows improved symmetry than CX implementation. By simultaneously optimizing both hardware and software aspects through careful algorithm design, efficient transpilation techniques, and DD sequences, it is possible to fully exploit the capabilities of near term quantum algorithms.

III. RESULTS ANALYSIS

This section delves into the examination of multiple factors that influence algorithm performance and DD effectiveness. These factors are classified into two main categories: hardware and algorithmic. More specifically, we thoroughly analyze the influence of circuit fidelity, schedule duration, and native gate set on the performance of

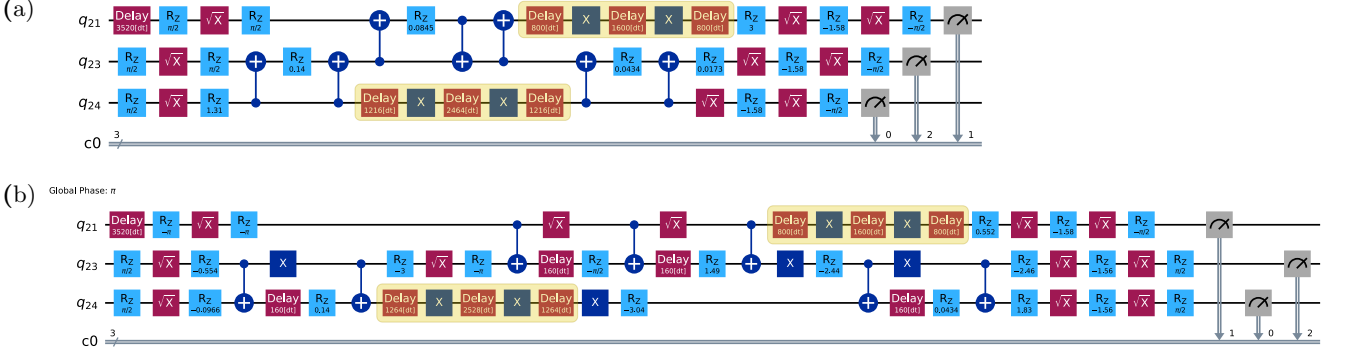


FIG. 3. Two implementations of a three-qubit QAOA: (a) CX-implementation, and (b) CZ-implementation, both are decomposed and optimized using Qiskit’s transpiler with optimization level 3. Highlighted yellow boxes represent CPMG sequences.

DD sequences. Furthermore, we explore the impact of algorithm implementation, choice of DD sequence, and level of optimization on algorithm performance and DD effectiveness. The objective of these analyses is to provide invaluable insights into the design and optimization of algorithm implementation for achieving efficient execution on quantum devices.

A. Impact of hardware factors

Our investigation begins by examining how hardware characteristics affect algorithm performance and DD effectiveness. The CPMG sequence is chosen for our study due to its widespread adoption and relative simplicity, allowing us to gain fundamental insights. We analyze these factors using extensive datasets. The experiments involve varying the qubit counts from 3 to 12 and investigating different combinations of algorithm implementations, including the CX and CZ versions of QAOA, as well as optimization levels 1 and 3 within the Qiskit framework. We conduct these experiments using eight QPUs, which consist of four 27-qubit devices: `ibmq_mumbai`, `ibmq_kolkata`, `ibm_cairo`, and `ibmq_ehningen`, and four 127-qubit devices: `ibm_kyoto`, `ibm_cusco`, `ibm_brisbane`, and `ibm_sherbrooke`. These extensive datasets provide a solid foundation for analyzing the impact of hardware factors on algorithm performance.

1. Circuit fidelity

We first explore the impact of circuit fidelity on the performance. The fidelity of a circuit qc , denoted as \mathcal{F}_{qc} , measures the agreement between the actual operation of a quantum circuit and its ideal operation. The circuit fidelity can be mathematically represented as

$$\mathcal{F}_{qc} = \prod_{G_s \in qc} f_{G_s} \prod_{G_t \in qc} f_{G_t} \prod_{G_m \in qc} f_{G_m}, \quad (12)$$

where f_{G_s} , f_{G_t} , and f_{G_m} denote fidelities of a single qubit gate G_s , a two qubit gate G_t , and the measurement G_m , respectively, in the circuit. We focus on circuits with fidelities exceeding 0.01 and present results in Fig. 4, including NAR_B , NAR_{DD} , NSP_B , NSP_{DD} , Δ_{NAR} , and Δ_{NSP} , as defined in Sec. II A 2. The measured data and the corresponding circuit fidelity are fitted using a linear function. The correlation coefficient C_r and p -value are computed to assess the quality of linear approximation. C_r quantifies the magnitude and direction of a linear relationship between two variables. It spans from -1 (indicating a perfect negative association) to 1 (indicating a perfect positive association), with 0 denoting no association. The absolute value of C_r indicates the correlation strength, which can be interpreted according to established conventions: very strong correlation ($|C_r|$ between 0.9 and 1.0), strong correlation ($|C_r|$ between 0.7 and 0.9), moderate correlation ($|C_r|$ between 0.4 and 0.7), weak correlation ($|C_r|$ between 0.2 and 0.4), and very weak correlation ($|C_r|$ between 0 and 0.2). However, it is important to note that correlation does not imply causation. The p -value is a complementary statistical measure that evaluates the strength of evidence against the null hypothesis of no correlation. A low p -value (typically below 0.05) suggests a statistically significant correlation, while a high p -value indicates that the correlation might be due to random chance. Linear fitting takes correlation a step further by determining the equation of a best fit line, enabling predictions based on the observed linear relationship.

Figure 4 depicts a general trend of improved algorithm performance with increasing circuit fidelity. DD sequences enhance both NAR and NSP on average. However, NSP exhibits a wider range of variation for a given circuit fidelity compared to approximation ratio, particularly at lower fidelities. Table II presents the average value, fitted function, correlation coefficient, and p -value for each metric. A stronger correlation is observed between NAR and circuit fidelity compared to NSP , suggesting a more pronounced dependence of NAR on fi-

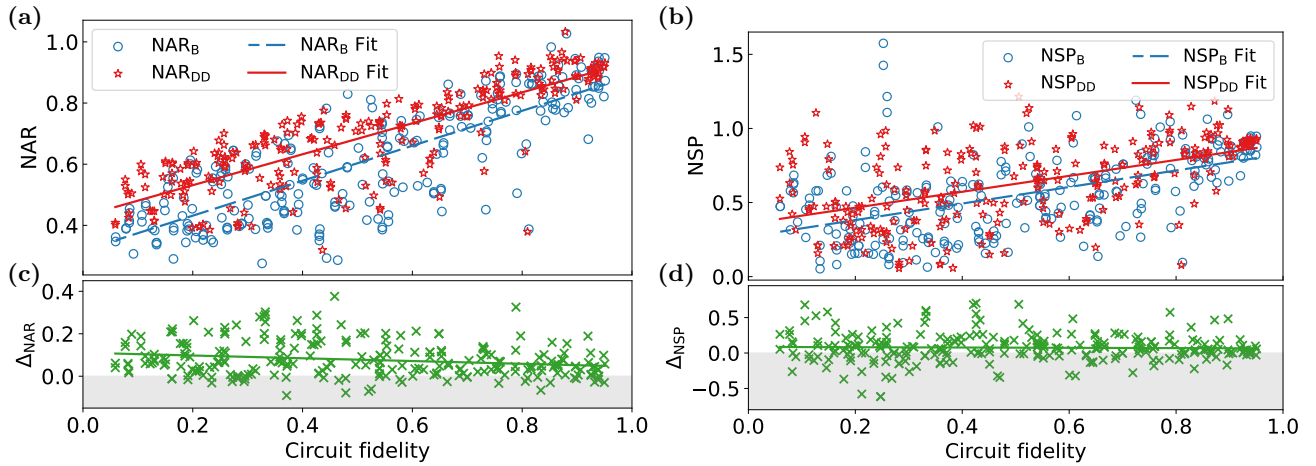


FIG. 4. Impact of circuit fidelity on algorithm performance and DD effectiveness. Higher values of NAR_B , NAR_{DD} , NSP_B , and NSP_{DD} indicate better performance on actual quantum devices. Values exceeding unity indicate that the performance achieved on the IBM quantum hardware surpasses the results obtained from the noise-free simulation. Positive values of Δ_{NAR} and Δ_{NSP} demonstrate improvements due to DD. The CPMG sequence is used for all data points. Each line in the graph represents a linear fit of the data. The reported $EMSR_{AR}$ and $EMSR_{SP}$ are 85.55% and 66.8%, respectively.

TABLE II. Parameters derived from the analysis of Fig. 4.

Metric	Mean	Fit function	Correlation coefficient	p-value
NAR_B	0.610	$y = 0.572x + 0.317$	0.809	0
NAR_{DD}	0.687	$y = 0.506x + 0.430$	0.827	0
NSP_B	0.556	$y = 0.558x + 0.270$	0.530	0
NSP_{DD}	0.631	$y = 0.537x + 0.358$	0.521	0
Δ_{NAR}	0.077	$y = -0.065x + 0.111$	-0.209	0.00075
Δ_{NSP}	0.075	$y = -0.021x + 0.086$	-0.027	0.66997

delity. In contrast, the correlation between Δ_{NSP} and circuit fidelity is very weak, as evidenced by the low value of C_r and high p -value. This suggests that the observed decrease in DD effectiveness might be due to random fluctuations or other factors not captured by circuit fidelity alone. The average improvement in NAR and NSP due to DD sequences is approximately 0.08. Moreover, the negative coefficients of the fitted lines for Δ_{NAR} and Δ_{NSP} suggest a potential decrease in DD effectiveness as circuit fidelity increases. Additionally, $EMSR$ calculated with the approximation ratio ($EMSR_{AR}$) is 85.55%, while $EMSR$ based on success probability ($EMSR_{SP}$) is 66.8%. On average, DD sequences demonstrate a success rate of 76.18% in improving algorithm performance, highlighting their robustness in mitigating errors in practical quantum algorithms.

2. Schedule duration

We now investigate the influence of schedule duration τ , and in particular the logarithmic transformation of schedule duration $\ln(\tau)$, on algorithm performance and DD effectiveness. Schedule duration reflects the total time required to execute a quantum circuit and depends

on the number and execution time of individual gates. Shorter durations potentially improve circuit fidelity by reducing the system's exposure to decoherence errors, but achieving them necessitates faster gates, which can be hardware limited.

Figure 5 depicts the impact of $\ln(\tau)$ on the defined metrics using the same datasets as in Fig. 4. We observe that the algorithm performance degrades with increasing schedule duration, while DD effectiveness improves. However, Δ_{NSP} exhibits larger fluctuations for longer durations, suggesting that while DD sequences mitigate decoherence errors, potentially improving performance at longer durations, they could also introduce other error mechanisms such as operation errors that counteract this improvement. Table III summarizes corresponding parameters. The coefficients of linear function for NAR_B , NAR_{DD} , NSP_B , and NSP_{DD} indicate a suppressed decay of performance with increasing schedule duration by applying DD sequences. The correlation coefficients between these metrics and $\ln(\tau)$ further support the effectiveness of DD sequences in reducing the dependence of performance (both NAR and NSP) on schedule duration. Δ_{NAR} exhibits a statistically weak correlation with $\ln(\tau)$, while Δ_{NSP} shows a very weak correlation. This observation aligns with the findings for circuit fidelity. However,

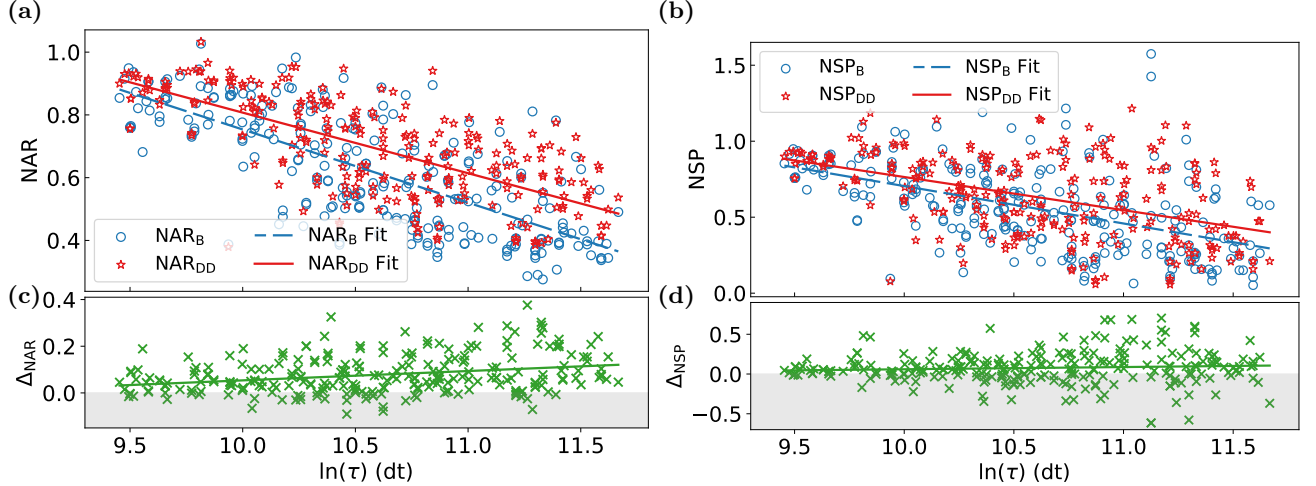


FIG. 5. Influence of logarithmic transformation of circuit schedule duration ($\ln(\tau)$) on algorithm performance and DD effectiveness with the same datasets as in Fig. 4.

TABLE III. Parameters derived from the analysis of Fig. 5.

Metric	Fit function	Correlation coefficient	p-value
NAR_B	$y = -0.234x + 1.124$	-0.732	0
NAR_{DD}	$y = -0.194x + 1.114$	-0.696	0
NSP_B	$y = -0.247x + 1.096$	-0.519	0
NSP_{DD}	$y = -0.219x + 1.111$	-0.468	0
Δ_{NAR}	$y = 0.040x - 0.010$	0.285	0
Δ_{NSP}	$y = 0.028x + 0.016$	0.079	0.20704

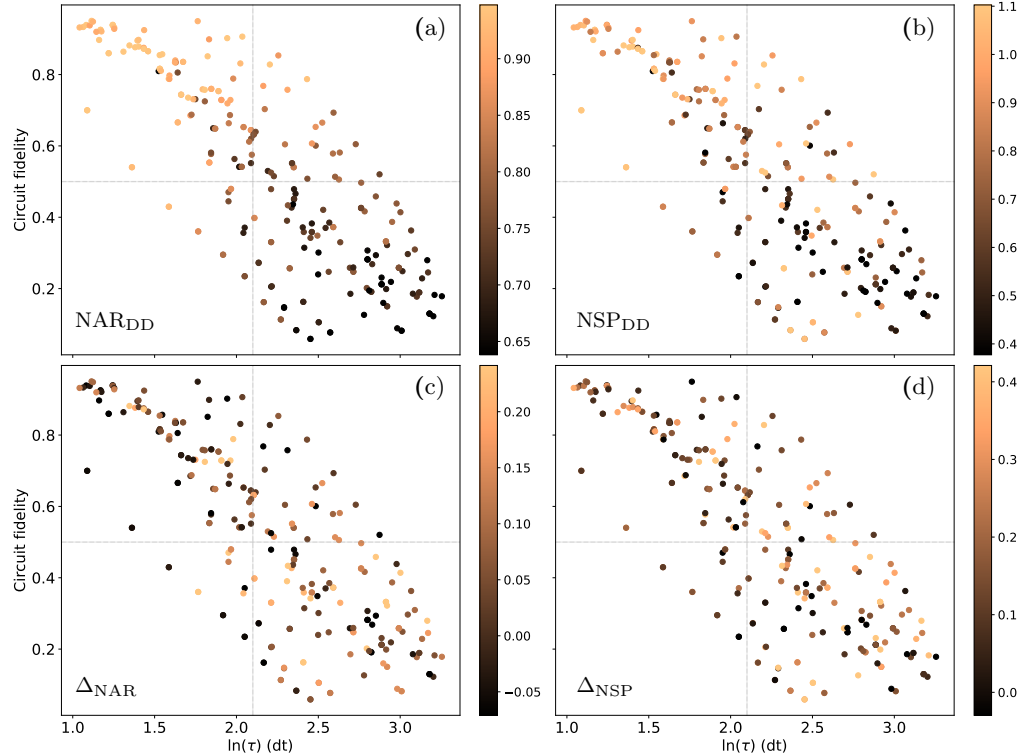


FIG. 6. Influence of circuit fidelity and $\ln(\tau)$ on algorithm performance and DD effectiveness: (a) NAR_{DD} , (b) NSP_{DD} , (c) Δ_{NAR} , and (d) Δ_{NSP} .

Δ_{NSP} appears more sensitive to schedule duration compared to circuit fidelity, as indicated by a larger absolute correlation coefficient ($|C_r|$) and lower p -value.

Figures 6(a-d) illustrate the impact of circuit fidelity and schedule duration on NAR_{DD} , NSP_{DD} , Δ_{NAR} , and Δ_{NSP} , respectively. As observed in Fig. 6(a), NAR_{DD} exhibits degradation with increasing logarithmic schedule duration ($\ln(\tau)$) and decreasing circuit fidelity. High performance is concentrated in the region where the schedule duration τ is below $e^{2.1} \text{ dt}$ and circuit fidelity surpasses 0.5. Conversely, low performance is primarily observed for τ exceeding $e^{2.1} \text{ dt}$ and fidelities below 0.5. A similar trend is evident for NSP_{DD} in Fig. 6(b). However, unlike NAR_{DD} , achieving a high NSP_{DD} value remains feasible even for longer schedule durations and lower fidelities. This suggests that NSP_{DD} is less sensitive to these factors compared to NAR_{DD} . Figures 6(c) and 6(d) further demonstrate the effectiveness of DD sequences, particularly at longer durations (higher $\ln(\tau)$). This is potentially due to the ability of DD sequences to mitigate decoherence errors that become more prominent at these timescales.

3. Native gate sets

This section explores the performance of quantum algorithms implemented on two distinct sets of IBM QPUs. The first set comprises four 27-qubit devices utilizing the CX gate as their native two qubit gate, while the second set consists of four 127-qubit devices employing the ECR gate as their native two qubit gate.

Benchmark results obtained from the two QPU sets are presented in Fig. 7. Table IV summarizes average values of metrics and parameters derived from the linear fits of these metrics against the number of qubits. As shown in Figs. 7(a) and 7(b), applying DD sequences generally improves NAR and NSP, respectively, for both native gate sets. The highest performance is achieved with $\text{NAR}_{\text{DD}}^{\text{ECR}}$ and $\text{NSP}_{\text{DD}}^{\text{ECR}}$, which leverages ECR-based QPUs and incorporates DD sequences. Moreover, QPUs utilizing ECR gate exhibit consistently higher baseline performance, $\text{NAR}_{\text{B}}^{\text{ECR}}$ and $\text{NSP}_{\text{B}}^{\text{ECR}}$, compared to those with CX gate, $\text{NAR}_{\text{B}}^{\text{CX}}$ and $\text{NSP}_{\text{B}}^{\text{CX}}$, even surpassing that with DD sequences, $\text{NAR}_{\text{DD}}^{\text{CX}}$ and $\text{NSP}_{\text{DD}}^{\text{CX}}$. This observation suggests that the selection of QPUs may be more critical for achieving optimal performance than relying solely on DD techniques. As shown in Figs. 7(c) and 7(d), DD effectiveness improves as the qubit count increases for both gate sets. Moreover, the CX gate set exhibits higher DD effectiveness than the ECR gate set. The circuit fidelity and $\ln(\tau)$ for each data point are presented in Figs. 7(e) and 7(f), respectively. ECR gate produces an overall higher circuit fidelity and lower schedule duration, potentially contributing to higher performance. The reported values of EMSR_{AR} and EMSR_{SP} are 92.5% and 72.5% for CX gate, respectively, resulting in an average 82.5% success rate. In comparison, these corresponding

values are 75% and 62.5%, respectively, for the ECR gate, leading to an average 68.75% success rate. This suggests that DD sequences are more robust in mitigating errors for the CX gate set compared to the ECR gate set.

The correlation coefficient presented in Table IV reveals a very strong native correlation between $\text{NAR}_{\text{DD}}^{\text{ECR}}$ and the number of qubits, compared to $\text{NAR}_{\text{B}}^{\text{ECR}}$. Similarly, a very strong negative correlation is observed between circuit fidelity and qubit count for both CX and ECR gate sets, indicating a significant decrease in circuit fidelity as the number of qubits increases. Moreover, we observe a weaker correlation between NSP and qubit number compared to NAR, implying that the impact of qubit count on success probability is less pronounced than its effect on approximation ratio. Additionally, the high p -values for $\Delta_{\text{NAR}}^{\text{ECR}}$ and $\Delta_{\text{NSP}}^{\text{ECR}}$ suggest that the effectiveness of DD sequences for ECR gates is more susceptible to random fluctuations.

Our demonstrations on eight IBM QPUs highlight the importance of circuit fidelity, schedule duration, and DD sequences in optimizing algorithm performance. As circuit fidelity decreases and schedule duration increases, DD sequences become increasingly important for mitigating errors and identifying optimal solutions. Furthermore, the results suggest that ECR-based QPUs offer advantages over CX-based QPUs. This is primarily due to the inherently shorter schedule durations and higher circuit fidelities associated with ECR gates. However, CX-based QPUs benefit more significantly from DD sequences in terms of error mitigation.

B. Impact of algorithmic factors

This section investigates the influence of algorithmic factors on the algorithm performance and DD effectiveness. We focus on three key aspects: algorithm implementations, DD sequence types, and circuit optimization levels.

1. Algorithm implementations

We compare the performance of CX and CZ implementations of QAOA on four 27-qubit IBM QPUs, as detailed in Sec. II C. The CPMG sequence is consistently utilized throughout this analysis. The results are presented in Fig. 8. As shown in Figs. 8(a) and 8(b), CZ implementation with DD sequences achieves the highest average values for both NAR ($\text{NAR}_{\text{DD}}^{\text{CZ}}$) and NSP ($\text{NSP}_{\text{DD}}^{\text{CZ}}$). However, for NSP at qubit counts exceeding 9, CZ implementation without DD sequences, $\text{NSP}_{\text{B}}^{\text{CZ}}$, outperforms that with DD sequences, $\text{NSP}_{\text{DD}}^{\text{CZ}}$, potentially due to the introduction of significant errors by DD sequences themselves. Furthermore, CX implementation exhibits an increasing DD effectiveness Δ_{NAR} and Δ_{NSP} , as the qubit number grows (Figs. 8(c) and 8(d)). Conversely, Δ_{NSP} for CZ

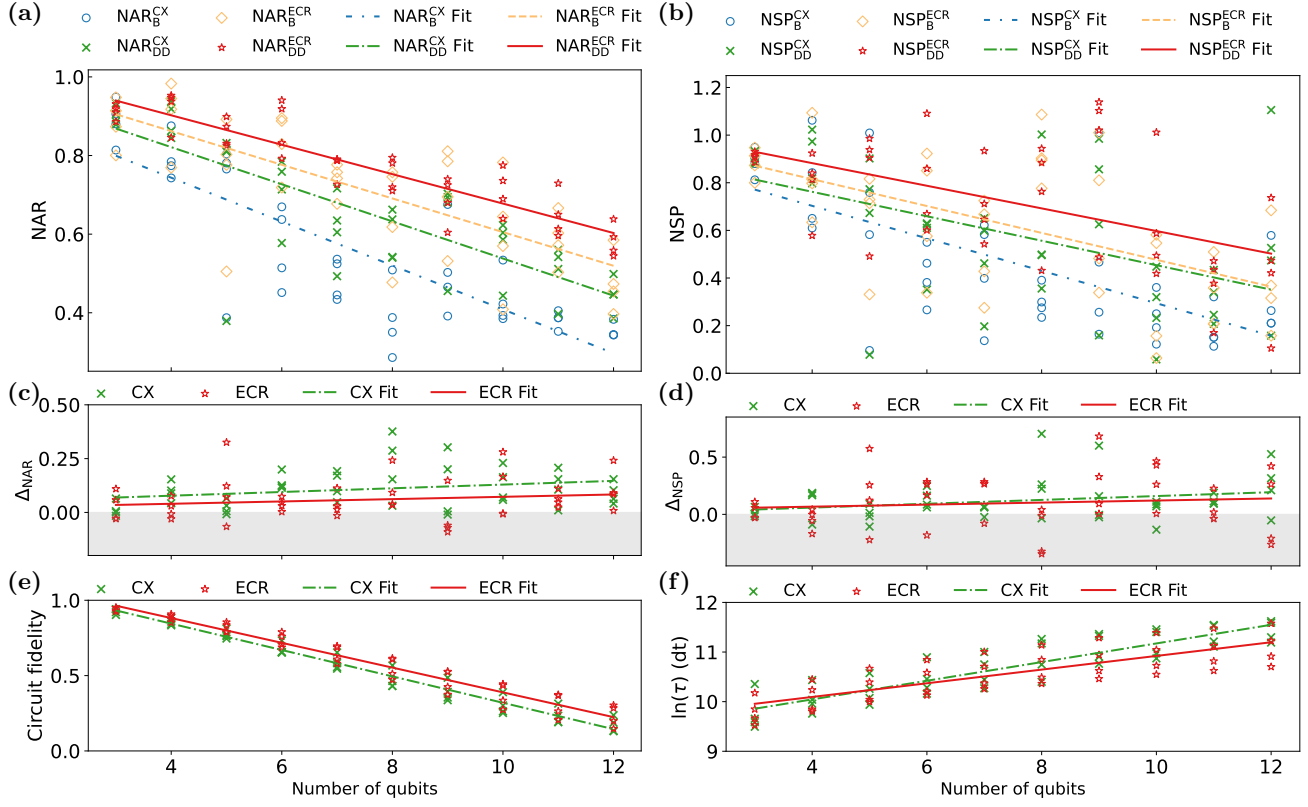


FIG. 7. Comparison of two hardware native gate sets: $\{\text{CX, ID, RZ, SX, X}\}$ and $\{\text{ECR, ID, RZ, SX, X}\}$, denoted as CX and ECR gate sets, respectively. Results obtained using four 27-qubit QPUs `ibmq_mumbai`, `ibmq_kolkata`, `ibm_cairo`, and `ibmq_ehningen` for the CX gate set, and four 127-qubit QPUs `ibm_kyoto`, `ibm_cusco`, `ibm_brisbane`, and `ibm_sherbrooke` for the ECR gate set: (a) NAR, (b) NSP, (c) Δ_{NAR} , (d) Δ_{NSP} , (e) circuit fidelity, and (f) $\ln(\tau)$. The CPMG sequence is used for all data points. Each line represents a linear fit to the corresponding data.

implementation, $\Delta_{\text{NSP}}^{\text{CZ}}$, slightly decreases with increasing qubit count. Additionally, EMSR_{AR} and EMSR_{SP} are consistently higher for CX implementation (92.5% and 80%, respectively) compared to CZ implementation (75% and 57.5%, respectively). This translates to an average EMSR of 86.25% for CX implementation and 66.25% for CZ implementation, suggesting higher robustness of DD sequences for CX implementation. Circuit fidelity and schedule duration are shown in Figs. 8(e) and 8(f), respectively. Both CX and CZ implementations exhibit comparable circuit fidelities. For a larger number of qubits, CX implementation even achieves slightly higher fidelities. Moreover, CX implementation demonstrates a consistently shorter schedule duration compared to CZ implementation. This difference in schedule duration is attributed to the increased number of single-qubit gates required by CZ implementation (details in Fig. 3).

Table V summarizes the average value of each metric along with the linear fit parameters extracted from Fig. 8. The negative coefficient associated with $\Delta_{\text{NSP}}^{\text{CZ}}$ suggests a decrease in DD effectiveness with an increasing qubit count for CZ implementation. Furthermore, correlation coefficients between NAR (NAR_B and NAR_{DD}) and qubit count reveal that applying DD sequences weakens

the correlation for CX implementation while strengthening it for CZ implementation. This trend is also observed for NSP_B and NSP_{DD} . An additional observation is the high p -values associated with $\Delta_{\text{NAR}}^{\text{CZ}}$ and $\Delta_{\text{NSP}}^{\text{CZ}}$ indicating the potential dominance of random fluctuations in these metrics for CZ implementation.

The results suggest that although CX implementation offers more advantages in terms of DD effectiveness, the higher performance of CZ implementation highlights the significance of circuit structure in executing QAOA. In certain instances, the inherent advantage of a more symmetrical circuit structure, as exhibited by CZ implementation, can outweigh the benefits of strong DD mitigation achieved with CX implementation. However, the optimal selection of gate decomposition ultimately relies on the specific algorithm being implemented, the hardware capabilities available, and the desired balance between overhead caused by DD and potential performance gains.

2. DD sequences

This section evaluates the performance of two DD sequences, CPMG and XY4, for mitigating decoherence er-

TABLE IV. Parameters derived from the analysis of Fig. 7.

Metric	Mean	Fit function	Correlation coefficient	p-value
NAR_B^{CX}	0.548	$y = -0.056x + 0.967$	-0.832	0
NAR_B^{DD}	0.656	$y = -0.047x + 1.010$	-0.812	0
NAR_B^{ECR}	0.712	$y = -0.043x + 1.033$	-0.766	0
NAR_{DD}^{ECR}	0.771	$y = -0.037x + 1.052$	-0.911	0
NSP_B^{CX}	0.464	$y = -0.068x + 0.976$	-0.678	0
NSP_{DD}^{CX}	0.582	$y = -0.051x + 0.967$	-0.504	0.00092
NSP_B^{ECR}	0.618	$y = -0.056x + 1.041$	-0.579	0.00009
NSP_{DD}^{ECR}	0.716	$y = -0.047x + 1.072$	-0.529	0.00044
Δ_{NAR}^{CX}	0.108	$y = 0.009x + 0.043$	0.27	0.09252
Δ_{NAR}^{DD}	0.059	$y = 0.005x + 0.019$	0.167	0.30429
Δ_{NAR}^{ECR}	0.118	$y = 0.017x - 0.008$	0.277	0.08407
Δ_{NAR}^{ECR}	0.098	$y = 0.009x + 0.031$	0.108	0.50688
Circuit fidelity (CX)	0.539	$y = -0.088x + 1.195$	-0.984	0
Circuit fidelity (ECR)	0.594	$y = -0.082x + 1.211$	-0.975	0
$\ln(\tau)$ (CX)	10.703	$y = 0.188x + 9.294$	0.891	0
$\ln(\tau)$ (ECR)	10.577	$y = 0.138x + 9.543$	0.791	0

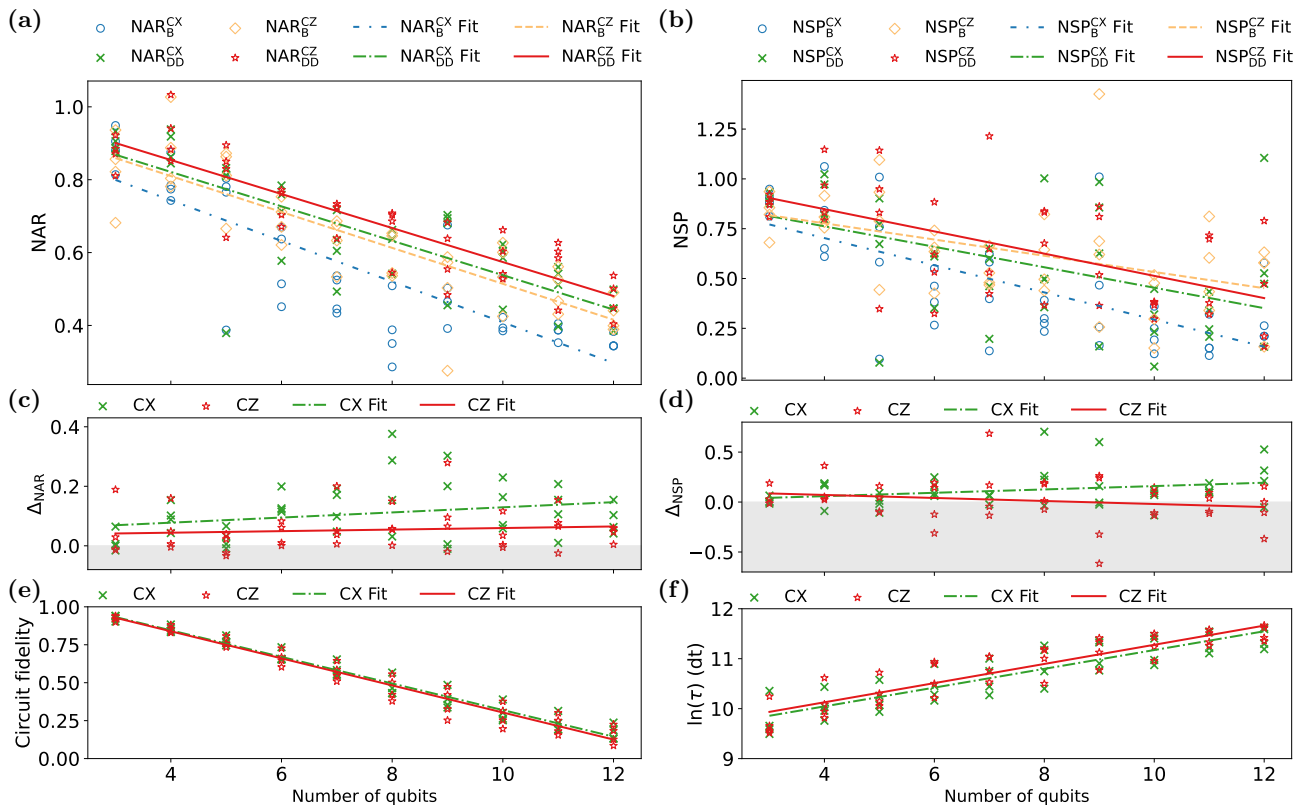


FIG. 8. Comparison of CX and CZ implementations of QAOA across four 27-qubit IBM QPUs ibmq_mumbai, ibmq_kolkata, ibmq_cairo, and ibmq_ehning. The CPMG sequence is used for all data points. Each line represents a linear fit of the data.

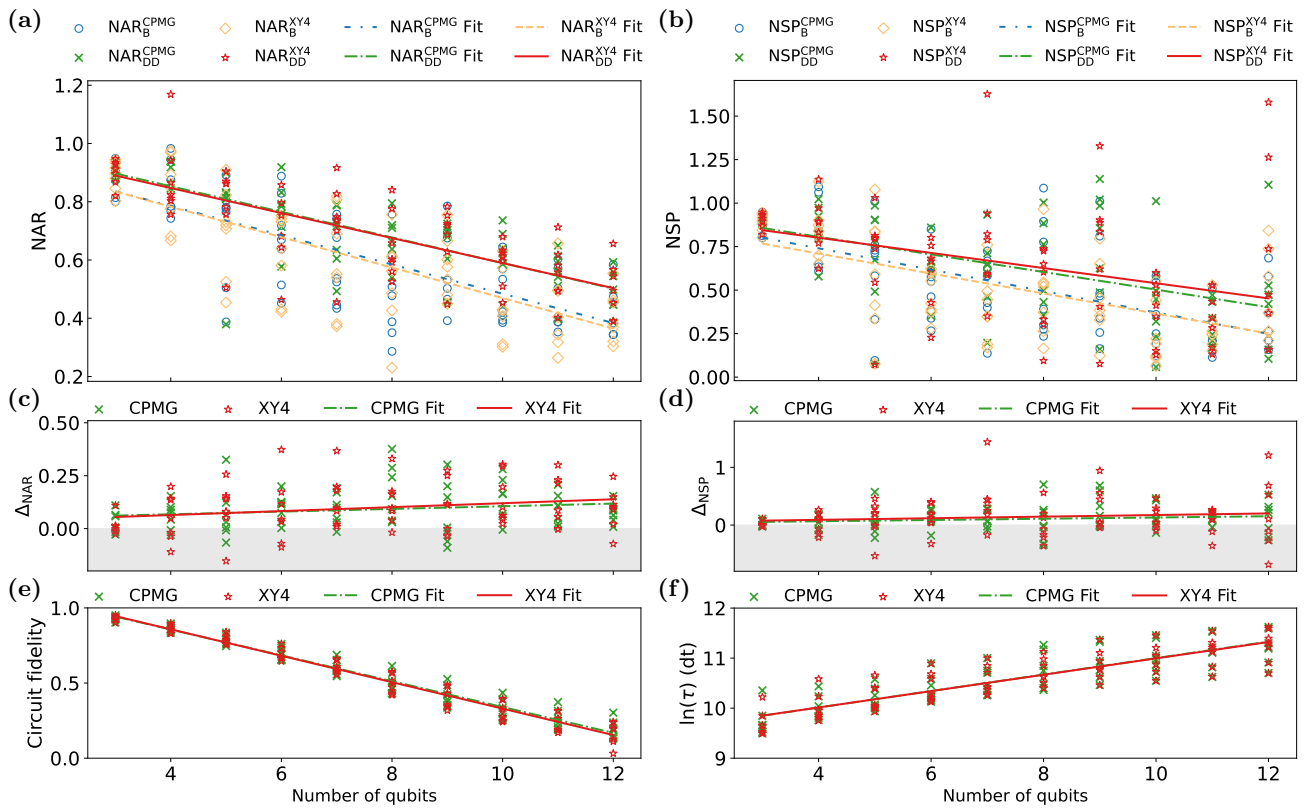
rors during QAOA execution with CX implementation. The evaluation leverages data from seven IBM QPUs. XY4, which employs four single qubit pulses, might be more effective for qubits with extended idle times than CPMG, which utilizes two single qubit pulses.

Figures 9(a) and 9(b) present the results for NAR and NSP, respectively. The data reveal that both CPMG

and XY4 contribute to improved algorithm performance. While CPMG and XY4 achieve comparable NAR values, XY4 exhibits better performance in terms of NSP for a larger number of qubits. However, the results for XY4 also display significant fluctuations. Δ_{NAR} and Δ_{NSP} , as shown in Figs. 9(c) and 9(d), demonstrate comparable performance between CPMG and XY4 for a small

TABLE V. Parameters derived from the analysis of Fig. 8.

Metric	Mean	Fit function	Correlation coefficient	p-value
NAR_B^{CX}	0.548	$y = -0.056x + 0.967$	-0.832	0
NAR_B^{DD}	0.656	$y = -0.047x + 1.010$	-0.812	0
NAR_B^{CZ}	0.638	$y = -0.049x + 1.007$	-0.850	0
NAR_B^{CZ}	0.691	$y = -0.047x + 1.041$	-0.885	0
NSP_B^{CX}	0.464	$y = -0.068x + 0.976$	-0.678	0
NSP_B^{DD}	0.582	$y = -0.051x + 0.967$	-0.504	0.00092
NSP_B^{CZ}	0.635	$y = -0.041x + 0.940$	-0.473	0.00208
NSP_B^{CZ}	0.653	$y = -0.056x + 1.071$	-0.589	0.00006
Δ_{NAR}^{CX}	0.108	$y = 0.009x + 0.043$	0.27	0.09252
Δ_{NAR}^{CZ}	0.053	$y = 0.003x + 0.034$	0.109	0.50206
Δ_{NSP}^{CX}	0.118	$y = 0.017x - 0.008$	0.277	0.08407
Δ_{NSP}^{CZ}	0.018	$y = -0.015x + 0.132$	-0.202	0.21130
Circuit fidelity (CX)	0.539	$y = -0.088x + 1.195$	-0.984	0
Circuit fidelity (CZ)	0.527	$y = -0.089x + 1.195$	-0.977	0
$\ln(\tau)$ (CX)	10.703	$y = 0.188x + 9.294$	0.891	0
$\ln(\tau)$ (CZ)	10.799	$y = 0.192x + 9.360$	0.901	0

FIG. 9. Comparison of CPMG and XY4 sequences across seven IBM QPUs `ibmq_mumbai`, `ibmq_kolkata`, `ibm_cairo`, `ibmq_ehningen`, `ibm_kyoto`, `ibm_cusco`, and `ibm_brisbane`. Each line represents a linear fit of the data.

number of qubits, while XY4 appears to be slightly more effective for a larger number of qubits. A key observation lies in the EMSR values. The reported $EMSR_{AR}$ and $EMSR_{SP}$ for CPMG are 84.29% and 75.71%, respectively, compared to 67.14% and 64.29% for XY4. This suggests a higher degree of robustness for the CPMG sequence. Figures 9(e) and 9(f) illustrate the circuit fidelity and

schedule duration, respectively, with comparable results observed for both CPMG and XY4.

As before, the data are fitted with a linear function. The resulting parameters for CPMG and XY4 sequences are summarized in Table VI. The coefficients of the linear function suggest that both CPMG and XY4 effectively suppress the decrease of NAR and NSP as the qubit

TABLE VI. Parameters derived from the analysis of Fig. 9.

Metric	Mean	Fit function	Correlation coefficient	p-value
$\text{NAR}_{\text{B}}^{\text{CPMG}}$	0.610	$y = -0.050x + 0.986$	-0.749	0
$\text{NAR}_{\text{DD}}^{\text{CPMG}}$	0.699	$y = -0.044x + 1.029$	-0.802	0
$\text{NAR}_{\text{B}}^{\text{XY4}}$	0.6	$y = -0.052x + 0.992$	-0.752	0
$\text{NAR}_{\text{DD}}^{\text{XY4}}$	0.697	$y = -0.043x + 1.019$	-0.750	0
$\text{NSP}_{\text{B}}^{\text{CPMG}}$	0.525	$y = -0.061x + 0.986$	-0.613	0
$\text{NSP}_{\text{DD}}^{\text{CPMG}}$	0.629	$y = -0.051x + 1.009$	-0.513	0.00001
$\text{NSP}_{\text{B}}^{\text{XY4}}$	0.509	$y = -0.057x + 0.940$	-0.591	0
$\text{NSP}_{\text{DD}}^{\text{XY4}}$	0.648	$y = -0.044x + 0.975$	-0.373	0.00148
$\Delta_{\text{NAR}}^{\text{CPMG}}$	0.09	$y = 0.006x + 0.042$	0.189	0.11748
$\Delta_{\text{NAR}}^{\text{XY4}}$	0.097	$y = 0.009x + 0.027$	0.23	0.05502
$\Delta_{\text{NSP}}^{\text{CPMG}}$	0.104	$y = 0.011x + 0.023$	0.144	0.23425
$\Delta_{\text{NSP}}^{\text{XY4}}$	0.139	$y = 0.014x + 0.035$	0.116	0.33818
Circuit fidelity (CPMG)	0.555	$y = -0.086x + 1.201$	-0.979	0
Circuit fidelity (XY4)	0.55	$y = -0.088x + 1.209$	-0.981	0
$\ln(\tau)$ (CPMG)	10.589	$y = 0.165x + 9.354$	0.851	0
$\ln(\tau)$ (XY4)	10.586	$y = 0.163x + 9.360$	0.858	0

count increases. The correlation coefficients and p -values suggest a stronger correlation between $\Delta_{\text{NAR}}^{\text{XY4}}$ and qubit count compared to $\Delta_{\text{NAR}}^{\text{CPMG}}$, $\Delta_{\text{NSP}}^{\text{XY4}}$, and $\Delta_{\text{NSP}}^{\text{CPMG}}$.

The results indicate that in principle, DD is generally recommended. The utilization of DD sequences expands the range of circuits where acceptable results can be achieved. For instance, QAOA can achieve an NAR value greater than 0.6 for a larger number of qubits when DD is employed. However, the effectiveness and robustness of DD sequences can vary. While XY4 yields slightly greater enhancements in algorithm performance, as indicated by NAR and NSP, CPMG demonstrates higher robustness, as evidenced by its higher EMSR values. This highlights the importance of considering not only performance improvements but also the trade-off with mitigation robustness when selecting a DD sequence.

3. Optimization levels

We investigate the influence of optimization levels on the performance and DD effectiveness using five IBM QPUs. Two optimization levels are considered: level 1 (Opt1) and level 3 (Opt3), representing the default and highest settings, respectively. The Qiskit's transpiler offers four optimization levels, ranging from 0 to 3. Level 0 performs no optimization, while level 3 performs the most extensive optimization. The default setting in Qiskit's transpiler is level 1, which performs light optimization. In comparison, level 2 performs heavy optimization. It is worth noting that different optimization levels do not affect the number of two qubit gates in our demonstration. This is because we are considering benchmark circuits that have already undergone the AOQMAP approach [44], which effectively ensures adherence to connectivity constraints and eliminates the need for additional SWAP gates. In our case, different optimization levels influence

the selected qubits for circuit execution and the count of single qubit gates, which affects the circuit fidelity and schedule duration. The CPMG sequence and CX implementation of QAOA are employed throughout this analysis.

Figure 10(a) and 10(b) demonstrate that Opt3 with DD sequences achieves the highest overall performance in terms of NAR and NSP. This is followed by Opt1 with DD sequences ($\text{NAR}_{\text{DD}}^{\text{Opt1}}$ and $\text{NSP}_{\text{DD}}^{\text{Opt1}}$), highlighting the importance of DD sequences in enhancing performance for both optimization levels. Without DD sequences, Opt3 outperforms Opt1 for all tested qubit counts in terms of NAR. However, for NSP, Opt3 exhibits an advantage only for a small number of qubits, with comparable performance achieved at larger qubit counts. The effectiveness of DD sequences is further explored in Figs. 10(c) and 10(d). Figure 10(c) shows that the average improvement in NAR due to DD sequences (Δ_{NAR}) is generally higher for Opt1 compared to Opt3. This suggests a stronger mitigating effect of DD sequences on performance degradation for Opt1. Similarly, Fig. 10(d) reveals that DD sequences are initially more beneficial for Opt1 in terms of NSP, with the advantage shifting towards Opt3 for larger qubit counts. Furthermore, the reported average EMSR_{AR} and EMSR_{SP} are 92% and 74% for Opt1, respectively, compared to 80% and 60% for Opt3. This indicates a potential advantage of DD sequences in terms of robustness for Opt1. It is important to note that Opt3 exhibits higher circuit fidelity (Fig. 10(e)) and shorter schedule duration (Fig. 10(f)), which are crucial for high algorithm performance.

The detailed linear fit parameters for the optimization levels are provided in Table VII. When DD sequences are applied, the decay of NAR is suppressed for Opt1, and the decay of NSP is suppressed for both Opt1 and Opt3 as the number of qubits increases. However, for Opt3, DD sequences appear to worsen the decay of NAR. This

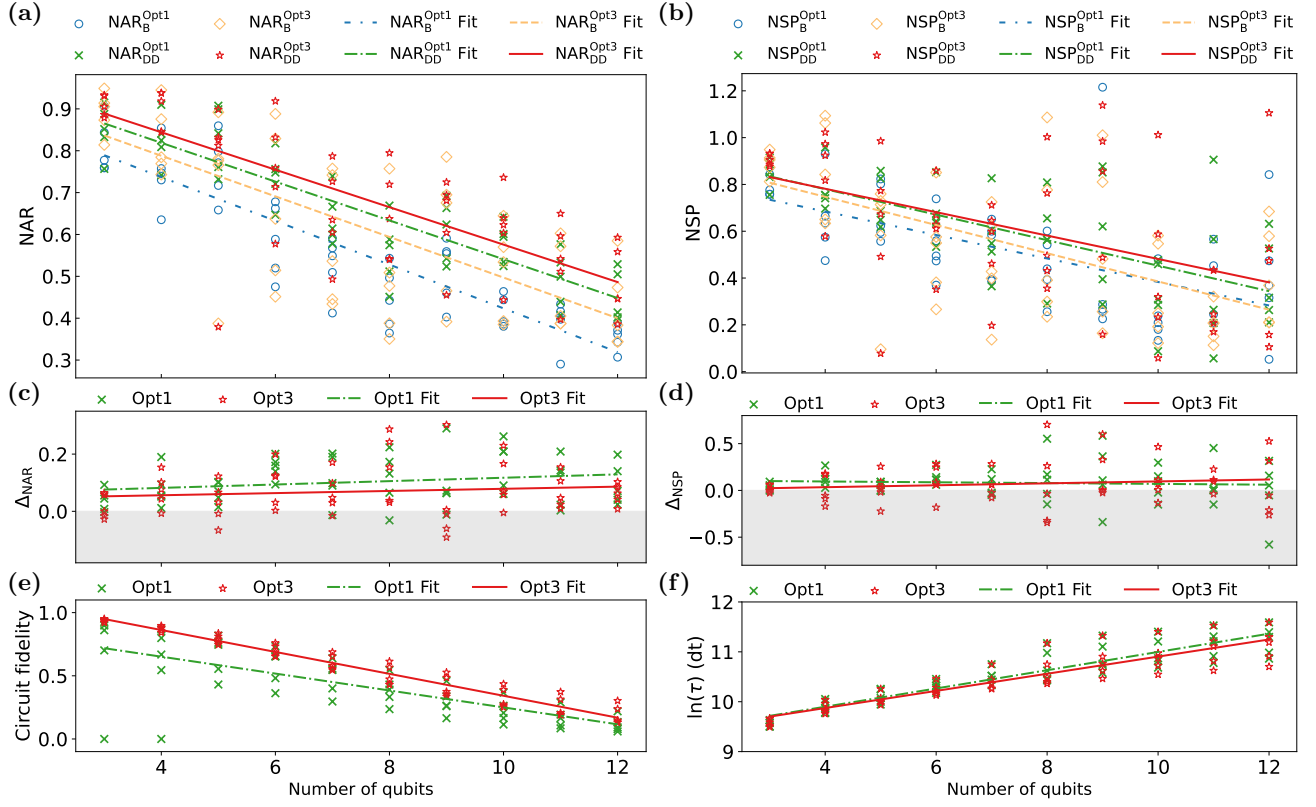


FIG. 10. Comparison of optimization level 1 (Opt1) and optimization level 3 (Opt3) across five IBM QPUs `ibmq_kolkata`, `ibmq_cairo`, `ibmq_ehningen`, `ibmq_cusco`, and `ibmq_kyoto`. The CPMG sequence is used for all data points. Each line represents a linear fit of the data.

TABLE VII. Parameters derived from the analysis of Fig. 10.

Metric	Mean	Fit function	Correlation coefficient	<i>p</i> -value
$\text{NAR}_B^{\text{Opt1}}$	0.554	$y = -0.052x + 0.946$	-0.891	0
$\text{NAR}_B^{\text{Opt1}}$	0.657	$y = -0.046x + 1.004$	-0.886	0
$\text{NAR}_B^{\text{Opt3}}$	0.509	$y = -0.050x + 0.885$	-0.596	0
$\text{NAR}_B^{\text{Opt3}}$	0.589	$y = -0.055x + 0.998$	-0.667	0
$\text{NSP}_B^{\text{Opt1}}$	0.525	$y = -0.061x + 0.986$	-0.613	0
$\text{NSP}_B^{\text{Opt1}}$	0.629	$y = -0.051x + 1.009$	-0.513	0.00001
$\text{NSP}_B^{\text{Opt3}}$	0.536	$y = -0.060x + 0.988$	-0.586	0.00001
$\text{NSP}_B^{\text{Opt3}}$	0.606	$y = -0.050x + 0.981$	-0.471	0.00056
$\Delta_{\text{NAR}}^{\text{Opt1}}$	0.103	$y = 0.006x + 0.058$	0.218	0.12785
$\Delta_{\text{NAR}}^{\text{Opt3}}$	0.069	$y = 0.004x + 0.041$	0.126	0.38513
$\Delta_{\text{NSP}}^{\text{Opt1}}$	0.08	$y = -0.004x + 0.113$	-0.065	0.65396
$\Delta_{\text{NSP}}^{\text{Opt3}}$	0.07	$y = 0.010x - 0.007$	0.136	0.34466
Circuit fidelity (Opt1)	0.417	$y = -0.067x + 0.919$	-0.729	0
Circuit fidelity (Opt3)	0.559	$y = -0.087x + 1.209$	-0.973	0
$\ln(\tau)$ (Opt1)	10.540	$y = 0.183x + 9.168$	0.919	0
$\ln(\tau)$ (Opt3)	10.475	$y = 0.172x + 9.186$	0.901	0

trend is also reflected in the corresponding correlation coefficients. These observations indicate that the effectiveness of DD sequences may decrease as the number of qubits increases, possibly due to errors accumulating within the sequences themselves. The correlation coefficient C_r is very low and the *p*-value is very high for

$\Delta_{\text{NSP}}^{\text{Opt1}}$, suggesting a very weak or no correlation between NSP with Opt1 and the number of qubits. Furthermore, Opt1 shows a stronger correlation with schedule duration, while Opt3 is more strongly correlated with circuit fidelity.

This analysis demonstrates a trade-off between the op-

timization level and DD effectiveness. While Opt3 offers superior overall performance with DD sequences, Opt1 exhibits higher DD effectiveness. Furthermore, DD sequences become increasingly beneficial for Opt3 at larger qubit counts for finding optimal solutions.

IV. DISCUSSION AND CONCLUSIONS

Our comprehensive study, conducted on eight IBM quantum devices, reveals that the application of dynamical decoupling (DD) sequences can significantly enhance the performance and robustness of algorithms on near term quantum devices. However, the effectiveness of DD sequences varies depending on hardware and algorithmic factors. A key finding is the observed inverse relationship between DD effectiveness and the original performance of algorithms without error mitigation. This implies that algorithms with higher inherent performance (measured without DD sequences) exhibit lower DD effectiveness. For instance, ECR-based QPUs offer superior native performance but reduced DD effectiveness compared to CX-based QPUs. Similarly, CZ implementation of QAOA exhibits higher native algorithm performance but lower average DD effectiveness compared to CX implementation. Moreover, optimization level 3 produces higher algorithm performance, but level 1 exhibits higher DD effectiveness. This inverse behavior can be attributed to the fact that algorithms with high performance typically have a lower intrinsic error rate, including the decoherence errors targeted by DD sequences. Furthermore, the introduction of DD pulse sequences can lead to new gate operation errors that decrease algorithm performance and potentially limit their effectiveness for certain algorithms.

DD sequences are typically more effective for algorithms with lower fidelity and longer schedule duration, but their impact on approximation ratio and success probability differs. The results indicate that while algorithms with lower circuit fidelity struggle to achieve high approximation ratio values, the application of DD sequences allows for achieving the simulated success probability. This finding suggests a potential methodology for obtaining the desired probabilities by studying different algorithm implementations and DD sequences, and selecting the measure that minimizes system energy.

One significant reason for the higher performance of algorithms on ECR-based QPUs is the inherently higher circuit fidelity and shorter schedule duration. However, another potential factor could be the inherent advantages of ECR gates. In these devices, ECR gates are only allowed for one direction, meaning that any two-qubit gate is directly decomposed into ECR gates with the same direction on the qubit pair. While the hardware-native CX gate also has a native direction, the reverse direction is supported, requiring additional single qubit gates and the hardware native CX gate for implementation. Directly decomposing algorithms into one-directional ECR gates could be more advantageous than using CX gates with

bidirectional capability at the gate level and then transforming them into native CX gates at the hardware pulse level. A similar trend is observed for CZ implementation, which produces a higher algorithm performance than CX implementation. The CX gate is directed, whereas the CZ gate is undirected, allowing for the decomposition of all two qubit gates with one directed CZ gate on one or more qubit pairs. Utilizing gates in the same direction could lead to a higher symmetry in the circuit, both in terms of single and two qubit gates, potentially contributing to error suppression and improved algorithmic performance. This highlights the importance of considering native gates at the pulse level and maintaining circuit structure symmetry during algorithm design.

In conclusion, this study demonstrates the significant impact of several factors on algorithm performance and the effectiveness of error mitigation across eight IBM QPUs. These factors include circuit fidelity, schedule duration, choice of hardware native gates, algorithm implementations, types of DD sequences, and optimization levels. Despite minimal performance variations between Carr-Purcell-Meiboom-Gill (CPMG) and XY4 sequences, XY4 exhibits a slight advantage in success probability for larger qubit counts. However, CPMG achieves a higher overall error mitigation success rate, suggesting potentially greater robustness. While the results highlight the general enhancement of algorithm performance and robustness through the use of DD sequences, achieving significantly improved performance relies more critically on factors such as high quality native gates of QPUs, symmetric algorithm implementation, and effective circuit optimization techniques. Therefore, a holistic approach that considers both hardware characteristics and software optimization strategies is important when designing quantum algorithms to maximize reliability and efficacy. This study underscores the importance of hardware considerations and circuit design in enhancing algorithm performance and robustness using DD sequences. These insights guide the development and optimization of other quantum applications. Future research directions include investigating the interplay between these factors when combining DD sequences with other error mitigation strategies, such as zero-noise extrapolation. Additionally, exploring the relationship between circuit symmetry and its effectiveness in suppressing errors could provide valuable insights. Extending this analysis to other quantum algorithms, such as the variational quantum eigensolver (VQE) and protocols for preparing Greenberger-Horne-Zeilinger (GHZ) states, holds promise for revealing the broader applicability of these findings.

ACKNOWLEDGMENTS

We acknowledge the use of IBM Quantum services for this work and to advanced services provided by the IBM Quantum Researchers Program. The views expressed are

those of the authors, and do not reflect the official policy or position of IBM or the IBM Quantum team. This work was funded in part by the Ministry of Economic

Affairs, Labour and Tourism Baden Württemberg, under the project QORA in the frame of the Competence Center Quantum Computing Baden-Württemberg.

[1] J. Preskill, Quantum computing in the nisq era and beyond, *Quantum* **2**, 79 (2018).

[2] Z. Cai, R. Babbush, S. C. Benjamin, S. Endo, W. J. Huggins, Y. Li, J. R. McClean, and T. E. O’Brien, Quantum error mitigation, *Rev. Mod. Phys.* **95**, 045005 (2023).

[3] D. Suter and G. A. Álvarez, Colloquium: Protecting quantum information against environmental noise, *Rev. Mod. Phys.* **88**, 041001 (2016).

[4] M. A. Ali Ahmed, G. A. Álvarez, and D. Suter, Robustness of dynamical decoupling sequences, *Phys. Rev. A* **87**, 042309 (2013).

[5] B. Pokharel, N. Anand, B. Fortman, and D. A. Lidar, Demonstration of fidelity improvement using dynamical decoupling with superconducting qubits, *Phys. Rev. Lett.* **121**, 220502 (2018).

[6] A. M. Souza, G. A. Álvarez, and D. Suter, Robust dynamical decoupling, *Philosophical Transactions of the Royal Society A: Mathematical, Physical and Engineering Sciences* **370**, 4748 (2012).

[7] G. De Lange, Z. Wang, D. Riste, V. Dobrovitski, and R. Hanson, Universal dynamical decoupling of a single solid-state spin from a spin bath, *Science* **330**, 60 (2010).

[8] J. Du, X. Rong, N. Zhao, Y. Wang, J. Yang, and R. Liu, Preserving electron spin coherence in solids by optimal dynamical decoupling, *Nature* **461**, 1265 (2009).

[9] D. Farfurnik, A. Jarmola, L. Pham, Z. Wang, V. Dobrovitski, R. Walsworth, D. Budker, and N. Bar-Gill, Improving the coherence properties of solid-state spin ensembles via optimized dynamical decoupling, in *Quantum Optics*, Vol. 9900 (SPIE, 2016) pp. 111–120.

[10] D. Farfurnik, A. Jarmola, L. M. Pham, Z.-H. Wang, V. V. Dobrovitski, R. L. Walsworth, D. Budker, and N. Bar-Gill, Optimizing a dynamical decoupling protocol for solid-state electronic spin ensembles in diamond, *Physical Review B* **92**, 060301 (2015).

[11] B. Merkel, P. Cova Fariña, and A. Reiserer, Dynamical decoupling of spin ensembles with strong anisotropic interactions, *Phys. Rev. Lett.* **127**, 030501 (2021).

[12] J. Medford, C. Barthel, C. Marcus, M. Hanson, A. Gossard, *et al.*, Scaling of dynamical decoupling for spin qubits, *Physical review letters* **108**, 086802 (2012).

[13] V. Tripathi, H. Chen, M. Khezri, K.-W. Yip, E. Levenson-Falk, and D. A. Lidar, Suppression of crosstalk in superconducting qubits using dynamical decoupling, *Physical Review Applied* **18**, 024068 (2022).

[14] J. Bylander, S. Gustavsson, F. Yan, F. Yoshihara, K. Harrabi, G. Fitch, D. G. Cory, Y. Nakamura, J.-S. Tsai, and W. D. Oliver, Noise spectroscopy through dynamical decoupling with a superconducting flux qubit, *Nature Physics* **7**, 565 (2011).

[15] M. J. Biercuk, H. Uys, A. P. VanDevender, N. Shiga, W. M. Itano, and J. J. Bollinger, Experimental uhrig dynamical decoupling using trapped ions, *Phys. Rev. A* **79**, 062324 (2009).

[16] B. Evert, Z. G. Izquierdo, J. Sud, H.-Y. Hu, S. Grabbe, E. G. Rieffel, M. J. Reagor, and Z. Wang, Syncopated dynamical decoupling for suppressing crosstalk in quantum circuits, arXiv preprint arXiv:2403.07836 (2024).

[17] J. Qiu, Y. Zhou, C.-K. Hu, J. Yuan, L. Zhang, J. Chu, W. Huang, W. Liu, K. Luo, Z. Ni, *et al.*, Suppressing coherent two-qubit errors via dynamical decoupling, *Physical Review Applied* **16**, 054047 (2021).

[18] H. Y. Carr and E. M. Purcell, Effects of diffusion on free precession in nuclear magnetic resonance experiments, *Phys. Rev.* **94**, 630 (1954).

[19] S. Meiboom and D. Gill, Modified Spin-Echo Method for Measuring Nuclear Relaxation Times, *Review of Scientific Instruments* **29**, 688 (2004), https://pubs.aip.org/aip/rsi/article-pdf/29/8/688/8343239/688_1_online.pdf.

[20] A. Maudsley, Modified carr-purcell-meiboom-gill sequence for nmr fourier imaging applications, *Journal of Magnetic Resonance* (1969) **69**, 488 (1986).

[21] G. A. Álvarez, A. M. Souza, and D. Suter, Iterative rotation scheme for robust dynamical decoupling, *Phys. Rev. A* **85**, 052324 (2012).

[22] L. Viola, E. Knill, and S. Lloyd, Dynamical decoupling of open quantum systems, *Phys. Rev. Lett.* **82**, 2417 (1999).

[23] A. M. Souza, G. A. Álvarez, and D. Suter, Effects of time-reversal symmetry in dynamical decoupling, *Phys. Rev. A* **85**, 032306 (2012).

[24] A. M. Souza, G. A. Álvarez, and D. Suter, Robust dynamical decoupling for quantum computing and quantum memory, *Phys. Rev. Lett.* **106**, 240501 (2011).

[25] G. S. Uhrig, Keeping a quantum bit alive by optimized π -pulse sequences, *Phys. Rev. Lett.* **98**, 100504 (2007).

[26] N. Ezzell, B. Pokharel, L. Tewala, G. Quiroz, and D. A. Lidar, Dynamical decoupling for superconducting qubits: A performance survey, *Phys. Rev. Appl.* **20**, 064027 (2023).

[27] E. Farhi, J. Goldstone, and S. Gutmann, A quantum approximate optimization algorithm, arXiv preprint arXiv:1411.4028 (2014).

[28] K. Blekos, D. Brand, A. Ceschini, C.-H. Chou, R.-H. Li, K. Pandya, and A. Summer, A review on quantum approximate optimization algorithm and its variants, *Physics Reports* **1068**, 1 (2024).

[29] A. Misra-Spieldenner, T. Bode, P. K. Schuhmacher, T. Stollenwerk, D. Bagrets, and F. K. Wilhelm, Mean-field approximate optimization algorithm, *PRX Quantum* **4**, 030335 (2023).

[30] L. Zhou, S.-T. Wang, S. Choi, H. Pichler, and M. D. Lukin, Quantum approximate optimization algorithm: Performance, mechanism, and implementation on near-term devices, *Physical Review X* **10**, 021067 (2020).

[31] M. P. Harrigan, K. J. Sung, M. Neeley, K. J. Satzinger, F. Arute, K. Arya, J. Atalaya, J. C. Bardin, R. Barends, S. Boixo, *et al.*, Quantum approximate optimization of non-planar graph problems on a planar superconducting processor, *Nature Physics* **17**, 332 (2021).

[32] S. Niu and A. Todri-Sanial, Effects of dynamical decoupling and pulse-level optimizations on ibm quantum com-

puters, *IEEE Transactions on Quantum Engineering* **3**, 1 (2022).

[33] P. Das, S. Tannu, S. Dangwal, and M. Qureshi, Adapt: Mitigating idling errors in qubits via adaptive dynamical decoupling, in *MICRO-54: 54th Annual IEEE/ACM International Symposium on Microarchitecture* (2021) pp. 950–962.

[34] C. Tong, H. Zhang, and B. Pokharel, Empirical learning of dynamical decoupling on quantum processors, arXiv preprint arXiv:2403.02294 (2024).

[35] Y. Ji, S. Brandhofer, and I. Polian, Calibration-aware transpilation for variational quantum optimization, in *2022 IEEE International Conference on Quantum Computing and Engineering (QCE)* (IEEE, 2022) pp. 204–214.

[36] P. Gokhale, A. Javadi-Abhari, N. Earnest, Y. Shi, and F. T. Chong, Optimized quantum compilation for near-term algorithms with openpulse, in *2020 53rd Annual IEEE/ACM International Symposium on Microarchitecture (MICRO)* (IEEE, 2020) pp. 186–200.

[37] F. Leymann and J. Barzen, The bitter truth about gate-based quantum algorithms in the nisq era, *Quantum Science and Technology* **5**, 044007 (2020).

[38] H.-L. Huang, X.-Y. Xu, C. Guo, G. Tian, S.-J. Wei, X. Sun, W.-S. Bao, and G.-L. Long, Near-term quantum computing techniques: Variational quantum algorithms, error mitigation, circuit compilation, benchmarking and classical simulation, *Science China Physics, Mechanics & Astronomy* **66**, 250302 (2023).

[39] J. J. Vartiainen, M. Möttönen, and M. M. Salomaa, Efficient decomposition of quantum gates, *Phys. Rev. Lett.* **92**, 177902 (2004).

[40] J. S. Baker and S. K. Radha, Wasserstein solution quality and the quantum approximate optimization algorithm: A portfolio optimization case study (2022), arXiv:2202.06782.

[41] S. Brandhofer, D. Braun, V. Dehn, G. Hellstern, M. Hüls, Y. Ji, I. Polian, A. S. Bhatia, and T. Wellens, Benchmarking the performance of portfolio optimization with qaoa, *Quantum Information Processing* **22**, 25 (2022).

[42] D. J. Egger, C. Gambella, J. Marecek, S. McFaddin, M. Mevissen, R. Raymond, A. Simonetto, S. Woerner, and E. Yndurain, Quantum computing for finance: State-of-the-art and future prospects, *IEEE Transactions on Quantum Engineering* **1**, 1 (2020).

[43] Y. Ji, K. F. Koenig, and I. Polian, Optimizing quantum algorithms on bipotent architectures, *Phys. Rev. A* **108**, 022610 (2023).

[44] Y. Ji, X. Chen, I. Polian, and Y. Ban, Algorithm-oriented qubit mapping for variational quantum algorithms, arXiv preprint arXiv:2310.09826 (2023).

[45] M. Cerezo, A. Arrasmith, R. Babbush, S. C. Benjamin, S. Endo, K. Fujii, J. R. McClean, K. Mitarai, X. Yuan, L. Cincio, *et al.*, Variational quantum algorithms, *Nature Reviews Physics* **3**, 625 (2021).

[46] Q. Contributors, Qiskit: An open-source framework for quantum computing, Zenodo: Geneva, Switzerland (2023).

[47] S. Sivarajah, S. Dilkes, A. Cowtan, W. Simmons, A. Edgington, and R. Duncan, t—ket>: a retargetable compiler for nisq devices, *Quantum Science and Technology* **6**, 014003 (2020).

[48] Y. Ji, K. F. Koenig, and I. Polian, Improving the performance of digitized counterdiabatic quantum optimization via algorithm-oriented qubit mapping, arXiv preprint arXiv:2311.14624 (2023).